MagBall: Magnetic Rollerball for Multi-Scale Contact Interactions on Diverse Surfaces

Chankyu (Charlie) Han
University of Washington
Seattle, Washington, USA
chankyu@uw.edu

Yuxuan Miao
University of Washington
Seattle, Washington, USA
ymiao6@uw.edu

Sen Zhang
University of Washington
Seattle, Washington, USA
szhang66@uw.edu

Yiyue Luo
University of Washington
Seattle, Washington, USA
yiyueluo@uw.edu

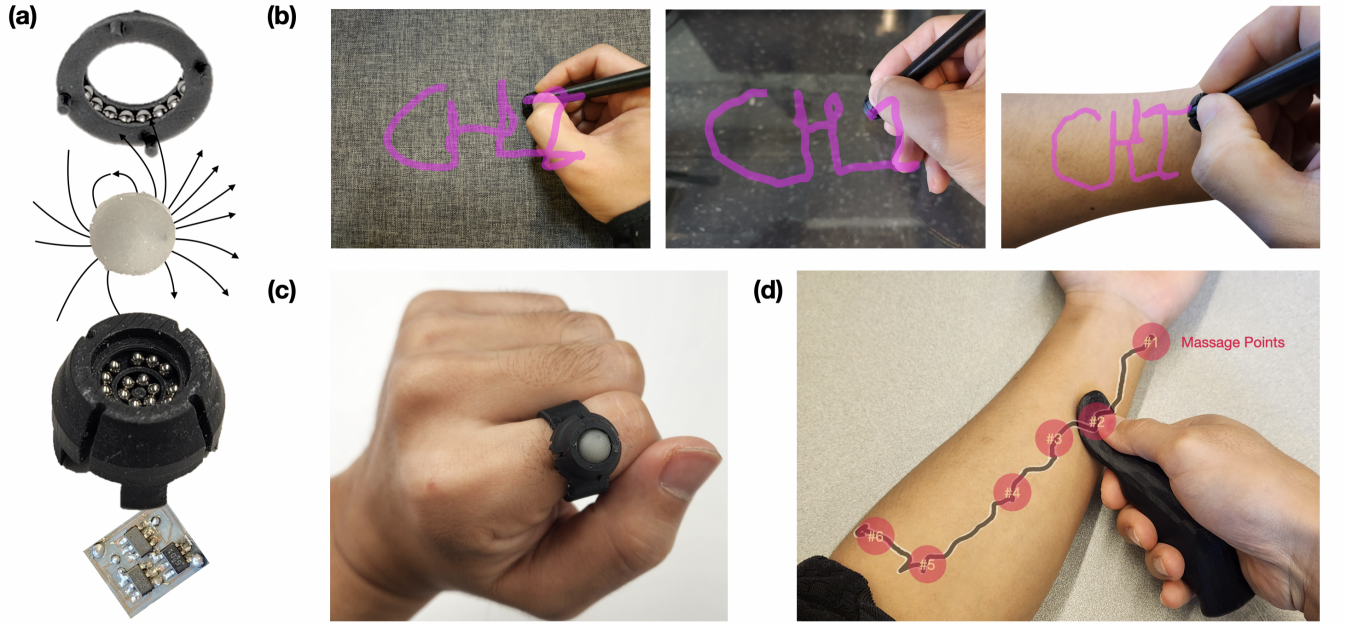

Figure 1: (a) MagBall is a compact input device that captures both precise displacement and force based on the change in magnetic field of a rolling magnet-embedded ball. We demonstrate applications of MagBall in (b) a surface-independent stylus pen, (c) a wearable trackball ring and (d) a smart massage tool.

Abstract

New tangible input techniques are transforming human-computer interaction. Point-contact devices such as joysticks or buttons are simple and scalable, but they capture limited spatial information. In contrast, surface-based contact interfaces such as touchpads provide richer spatial input but require larger instrumented surfaces. We present MagBall, a magnetic-ball sensor that captures fine-grained interactions, including displacement and force, through the rotation of a magnet-embedded ball over a 3D Hall-effect sensor array. Our design localizes diverse physical interactions to a single point-contact yet operates at multiple scales from millimeters to meters. Our machine learning models can infer the displacement and force with root-mean-squared errors of 0.15 mm and 0.67 N. Furthermore, our device supports interactions across diverse surfaces such as glass, metal and human skin, without additional instrumentation. We demonstrate applications in stylus pens, wearable trackballs and smart massage tools, which naturally aligns with the rolling mechanism of MagBall.

CHI '26, Barcelona, Spain

ACM ISBN 979-8-4007-2278-3/26/04
https://doi.org/10.1145/3772318.3791366

Keywords

Input Techniques, Tangible Interaction, Magnetic Sensing, Surface-Independent Input, Rolling Interaction, Hall-Effect Sensors

ACM Reference Format:
Chankyu (Charlie) Han, Yuxuan Miao, Sen Zhang, and Yiyue Luo. 2026. MagBall: Magnetic Rollerball for Multi-Scale Contact Interactions on Diverse Surfaces. In *Proceedings of the 2026 CHI Conference on Human Factors in Computing Systems (CHI '26), April 13–17, 2026, Barcelona, Spain.* ACM, New York, NY, USA, 17 pages. https://doi.org/10.1145/3772318.3791366

1 Introduction

Tangible input interfaces are essential for human–computer interaction, as they serve as the medium to digitize physical actions and convey information [10, 51]. The size of existing input devices often scales with the size of the interaction space, creating a fundamental trade-off between device compactness and interaction richness. Point-contact devices, such as joysticks and buttons [14, 38, 52], are compact and easy to integrate into diverse tools, but they typically capture only limited spatial information such as click or pressure at discrete positions. Surface-based devices, such as capacitive touchpads [26, 39, 47], support a richer set of gestures and multi-touch inputs. However, the interaction is still confined to instrumented surfaces, where sensing cost and complexity grow with resolution and interaction area. Moreover, the additional instrumentation increases size and complexity, making integration into diverse objects more difficult. There is growing demand for compact tangible input devices that can seamlessly transform ordinary objects into interactive devices, capturing interactions in their everyday settings.

In particular, rolling mechanisms can expand interaction space while keeping devices compact. By mapping continuous motion into localized rotation, a rolling element decouples device size from interaction scale. For example, commercial trackball mice [3, 4] exploit the rolling principle, allowing users to navigate large computer screen with small hand movements. On a larger scale, Disney's HoloTile floor [53] uses omnidirectional rotating tiles to let users walk or run in expansive virtual worlds within a confined physical space. Rolling thus provides a pathway to design input devices that are both compact and expressive, enabling large-scale interaction through localized physical interactions.

Inspired by the rolling mechanism, we present MagBall, a compact point-contact input device that digitizes multi-scale surface-independent interaction (Fig. 1). MagBall senses interactions through the change of magnetic fields, generated by movement of a magnet-embedded ball over an array of Hall-effect sensors. MagBall integrates all components in a single compact unit with the sizes of 13 mm x 13 mm x 10 mm, supporting both fine-grained and large-scale interactions, ranging millimeters to meters. Using machine-learning models, we estimate both 2D displacement and applied force with root-mean-squared errors (RMSE) of 0.15 mm and 0.67 N. Our design takes inspiration from ballpoint pens: just as a pen tip translates hand motions into continuous strokes, MagBall digitizes interactions through a single rolling contact point. Different from commercial stylus pens and touchpads, which require capacitive or electromagnetic resonance sensing grids, MagBall functions over any type of surfaces such as glass, metal, fabric and skin. Moreover, MagBall can be seamlessly embedded into everyday objects featuring rolling mechanisms, such as trackballs, stylus pens, and massage tools.

Our contributions are as follows:

- We design and implement MagBall, an omni-directional rolling device that enables multi-scale surface-independent interactions.
- We explore the design space via static magnetic field simulation.
- We develop a machine-learning pipeline to estimate 2D displacements and force from MagBall measurements.
- We experimentally evaluate sensing performance and estimation accuracy for both displacement and force.
- We quantitatively evaluate performance on various ordinary surfaces through an experiment and a user study.
- We demonstrate applications of our system in a surface-independent digital pen, a wearable trackball ring, and a smart massage tool.

2 Related Work

This work presents a point-contact magnetic interface for multi-scale contact-interactions on diverse surfaces based on rolling mechanism. To contextualize our research, we examine prior work in these key areas: tangible input techniques, magnetoactive interactive interfaces, trackballs and passive-surface interaction.

2.1 Tangible Input Techniques

Tangible input techniques have long been a focal topic in human-computer interaction, converting diverse physical signals such as pose and pressure into digital inputs. The size and expressivity of the device are two aspects that are commonly evaluated and traded off. Large devices leverage their volume or area to capture rich information [11, 20, 34, 45, 54–56]. For example, researchers instrumented tables, walls, and other large surfaces with sensor arrays to enable rich bimanual and multiobject manipulation [17, 21, 43]. Although such systems support large interaction, they typically require hardware that covers entire surfaces. Furthermore, it is difficult to capture fine-grained interaction unless the sensing grid gets much denser, leading to high deployment cost.

To improve portability, tangible input techniques have emerged at the personal device scale [13, 23, 35, 63]. This line of work allows more subtle interaction on or near smaller surfaces. Capacitive approaches [49, 50, 57, 61] allow devices to recognize props and their poses, and magnetic approaches achieve robust tracking on and just above surfaces [6, 28, 31, 60]. However, these devices generally must be paired with instrumented surfaces at the size of portable devices, which limits spatial expressivity.

Our work addresses aforementioned trade-off between device size and spatial expressivity by introducing a compact tangible input device that leverages rolling mechanism to transform localized rotation into multi-scale spatial interaction on diverse surfaces.

2.2 Magnetoactive Interactive Interfaces

Magnetic materials enable custom interactive experiences. By tailoring magnetization patterns and spatial arrangements of magnets, these systems generate magnetic field measurements that are sensitive to desired physical information such as displacement and force (Table 1). Because a magnet produces a 3D spatial magnetic field, magnets are frequently used to create fine-grained 3D spatial interaction [15, 16, 18, 27, 59, 62]. MagPen [19] uses a pen with an

System Name	Sensing Principle	Force Sensing	Unconstrained Interaction Space	Yaw Compensation	Compatible Surface Diversity			Off-contact Tracking	Sensor Size
					Rigid, Flat	Rigid, Curved	Soft		
GaussSense [30]	magnetic	✓	✗	✓	✓	✗	✗	✓	small
MagPen [19]	magnetic	✓	✗	✓	✓	✓	✓	✓	small
Berkelman et al. [2]	magnetic	✗	✗	✓	✗	✗	✗	✓	large
Flashpen [48]	optical flow	✗	✓	✓	–	✗	✗	✓	small
DeltaPen [37]	optical flow + piezoresistive	✓	✓	✓	–	✗	✗	✓	small
OptiBasePen [9]	optical flow + infra-red	✓	✓	✓	–	✗	✗	✓	large
Handwriting-Assistant [5]	inertial measurement unit	✗	✓	✓	✓	✗	✗	✓	small
Analogue trackball [3]	rotary encoders	✗	✓	✗	✓	✓	✓	✗	large
Optical trackball [4]	optical flow	✗	✓	✓	✓	✓	✓	✗	large
Magnetic trackball [41]	magnetic encoders	✗	✓	✗	✓	✓	✓	✗	small
Anoto pen [1]	camera	✓	✗	✓	✗	✗	✗	✓	small
MagBall (ours)	magnetic	✓	✓	✓	✓	✓	✓	✗	small

Table 1: Comparison of MagBall with other magnetic interfaces, passive-surface styluses, and commercial trackballs. – is used for optical-based systems that could work on different surfaces but do not provide any evaluation on diverse surface such as transparent one, where failure is expected. Sensor sizes indicate whether the sensing components fit within a pen form factor.

embedded magnet and a smartphone's built-in 3D magnetometer to recognize various gestures and contact strokes of the pen with smartphone. However, magnetic field strength decays cubically with distance, which limits the interaction space. One approach to expand this space is to deploy an array of distributed magnetometers [17, 22, 28–30, 32, 33]. However, the cost and complexity of deployment grows with the interaction volume. Yan et al. [58] mitigated this limitation by designing careful magnetization patterns and leveraging machine-learning-based super-resolution to reduce the number of required sensors. Nevertheless, the spatial expressivity of such systems remains fundamentally constrained by the overall size of the magnetometer array.

Our work preserves the compactness while overcoming limited interaction space. We minimize the number of Hall-effect sensors to reduce overall size of the system. The sensors move along with the device enabling unbounded interaction space. The user's unbounded movements are translated into rotational motion of MagBall, which is effectively captured by a Hall-effect sensor array inside the device. In summary, our approach provides an interaction that satisfies both a small device footprint and a large effective interaction area.

2.3 Trackballs and Passive-Surface Interaction

Trackballs are the closest relatives to our approach (Table 1). Traditional analogue trackballs [3] employ an omnidirectional ball supported by two or four rollers whose rotation is measured using rotary encoders. Optical trackballs [4] instead track the motion of a patterned ball using an optical-flow sensor. While effective as mouse replacements, commercial designs remain several centimeters in size, which is too large for wearable or mobile applications.

Efforts toward miniaturized magnetic trackballs for mobile devices [41] have reduced the form factor using compact magnetic encoders. However, these roller-based mechanisms share a fundamental limitation: they cannot resolve yaw rotation. Although yaw is insignificant in typical cursor-control tasks, it is intrinsic to sliding-contact interactions in real-world scenarios. For example, when drawing with a pen, small rotations around the pen's long axis occur naturally. Without resolving yaw rotation, it is not possible to infer relative displacement between sliding surface accurately from a single-body sensing system (more details in Section 7.1).

Complementary work explores passive-surface interactive pens, which use optical-flow sensors to track motion over uninstrumented surfaces [9, 37, 48] (Table 1). These systems capture displacement by estimating frame-to-frame image motion, which includes yaw information, and achieve high accuracy on an ordinary table. However, optical-flow approaches fail on transparent or reflective materials such as glass and mirrors, and their accuracy degrades on soft, deformable or irregularly curved surfaces such as skin, fabric and cushions due to changing surface geometry.

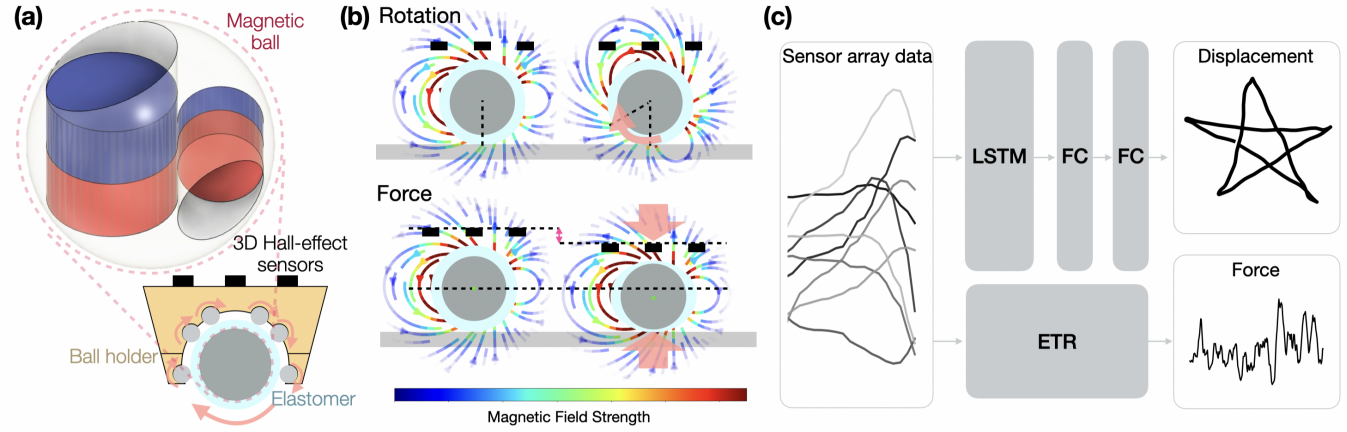

Figure 2: System overview. (a) The sensor consists of a multi-magnet core within an elastomer shell, which rotates freely in a ball holder over a 3D Hall-effect sensor array. (b) User-applied rotation and normal force changes the magnetic field patterns detected by the sensors. (c) Signals from 9-channel Hall-effect sensors are processed by machine learning models, Long Short-Term Memory (LSTM), Fully-Connected layer (FC), Extra Trees Regressor (ETR), to estimate corresponding 2D displacement and applied force.

MagBall bridges and expands these two concepts, reinventing compact trackball for general sliding-contact sensing compatible with diverse surfaces. Unlike trackballs, it is explicitly designed to resolve yaw rotation through an asymmetric magnetic field formation, validated in both simulation and experiment. Unlike optical-flow pens, MagBall does not assume any particular surface geometry, material or rigidity. Therefore, MagBall robustly operates across diverse real-world surfaces and remains stable even in the presence of weak incidental magnets. Only strong magnetic interference, which is rare in everyday environments, degrades performance. Consequently, MagBall extends beyond cursor control and stylus input to support a broader class of sliding-contact interactions such as monitoring massage procedures.

3 System Overview

Our sensing principle relies on variations in the near-field magnetic field generated by embedded permanent magnets. As shown in Fig. 2(a), MagBall is inspired by ballpoint pens, consisting of a free-rolling magnetic ball tip mounted in a ball holder. The magnetic ball is a rigid sphere encapsulated by an elastomer layer and embedded with two permanent magnets of different sizes (K&J Magnetics). The ball holder keeps the magnetic ball in place and allows smooth omnidirectional rolling via small bearing balls (1.5 mm diameter). Three 3D Hall-effect sensors (TMAG5273, Texas Instruments) are mounted on the ball holder. When the magnetic ball rolls or compresses against external surfaces, such as a user's skin or a tabletop, the embedded magnets move or rotate, and generate time-varying 3D magnetic fields. These signals are captured by the Hall-effect sensors (Fig. 2(b)). The signal varies uniquely with different ball orientations and applied forces. When the magnetic ball rotates along a fixed axis, the Hall-effect sensor outputs periodic signals, with each channel exhibiting distinct patterns. These characteristic patterns change when the ball is rotated around another axis, which includes yaw rotation as well. When force is applied, the magnetic ball moves closer to the Hall-effect sensors, and the magnitudes of signals from every channel increase due to the stronger magnetic field. Because the sensors are positioned only millimeters away from magnets, these variations on orientations and positions of the magnetic ball produce measurable variations in the Hall-effect sensor readings. The raw sensor data is processed by a machine learning pipeline to estimate both displacement and force in real time (Fig. 2(c)). Here, the displacement refers to 2D motion of the contact point on the surface as MagBall rolls.

4 Design and Implementation

We perform static magnetic field simulation to efficiently explore the design space of MagBall. Simulations enable precise and high-spatial-resolution measurements at sub-millimeter scale, which are difficult to achieve experimentally. They also enable rapid iterations, allowing comprehensive exploration of the design space. We identify optimized design parameters in magnet configuration, elastomer thickness, number of Hall-effect sensors and sensor spacing.

4.1 Design Exploration via Simulation

We utilized Magpylib [40], an open-source Python library for static magnetic field simulation. It computes 3D magnetic fields at specified spatial coordinates given a magnet configuration, including size, shape, polarization strength, orientation, and position.

In our simulation setup, we define the magnet configuration and fix its center at the origin, representing a stationary magnetic ball. We are able to simulate the 3D magnetic field vector at any sampled point in the surrounding 3D space. To emulate the sensing process, the Hall-effect sensors are arranged on a virtual PCB plane that moves along different positions around the fixed magnet (Fig. 3). Each real-world sensor measurement corresponds to the 3D magnetic field vector at the corresponding sensor coordinates in the simulation. Although the simulation rotates the sensors around a fixed magnet, this is equivalent to the real deployment scenario in

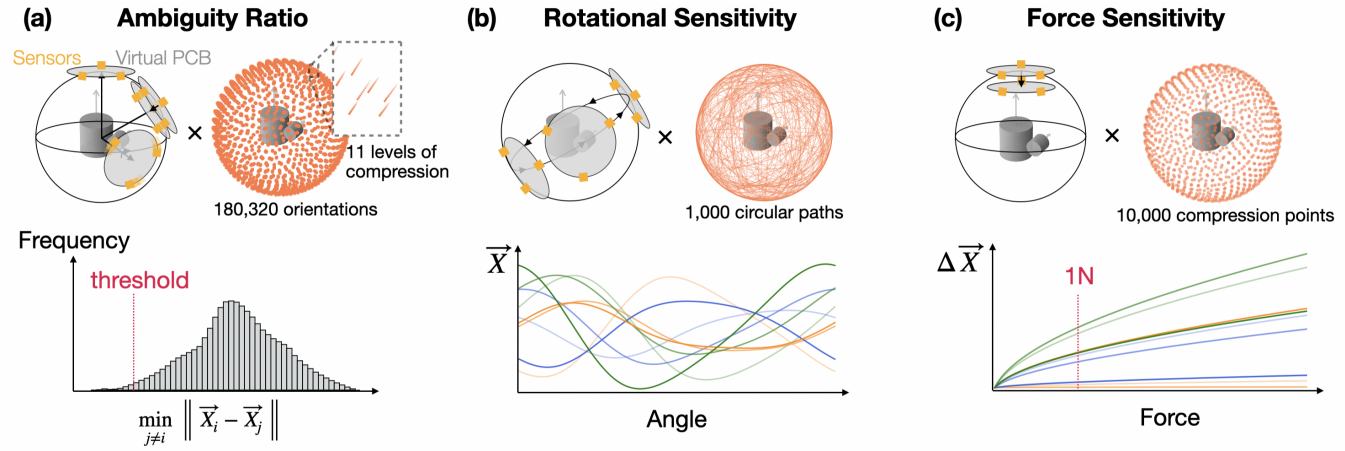

Figure 3: Evaluation metrics for design exploration. (a) For ambiguity ratio, sensor measurements $\vec{X}$ were collected at 180,320 orientations across 11 compression levels. The plot shows a distribution of the minimum measurement differences for all poses, used to quantify the ambiguity ratio. (b) Rotational sensitivity was evaluated with measurements at 1,000 random circular paths. The plot shows sensor readings along one circular path. (c) Force sensitivity was evaluated at 10,000 compression points. The plot shows sensor readings at one compression point. Note that only 10% of orientations, circular paths, and compression points are drawn in orange dots or lines for clear visualization.

which the sensors remain stationary and the magnetic ball rotates. To simulate yaw, the virtual PCB is spun around at each point along radial axis. To simulate compression by applied forces, the virtual PCB plane progressively moves closer to the fixed magnets. In other words, by varying the position and orientation of the virtual PCB, we simulated the embedded magnetic ball in various poses, defined by both its orientation and position.

We evaluate the performance of our system with different design parameters based on three metrics: ambiguity ratio, rotational sensitivity and force sensitivity. All of them can be extracted from simulation.

4.1.1 Ambiguity Ratio. A key criterion for robust sensing is minimizing signal ambiguity, meaning each pose of the magnetic ball should correspond to a unique sensor reading [42]. To quantify performance of our sensor, we define the ambiguity ratio as the proportion of magnetic ball poses that yield indistinguishable sensor readings. A high ambiguity ratio indicates that the sensor reading cannot uniquely resolve certain poses, leading to errors in displacement and force estimation. An ideal design should minimize the ambiguity ratio, ensuring the robustness and accuracy of MagBall.

We obtained simulated sensor readings at a dense and uniformly distributed set of approximately 2,000,000 poses, with 180,320 magnetic ball orientations including 10 yaw rotations at each point and 11 compression levels (Fig. 3(a)). Compression levels are spaced at 0.05 mm intervals, resulting in a maximum compression of 0.5 mm.

Ambiguity ratio is calculated by Eq. 1.

$$Ambiguity\ Ratio = \frac{\text{count}\{i, \min_{j \neq i} \left\| \vec{X}_i - \vec{X}_j \right\|_2 < threshold\}}{N} \quad (1)$$

where $\vec{X}_i$ is the sensor array measurements at pose i and N is total number of poses. Two sensor readings are considered ambiguous if their difference is within the noise threshold of the Hall-effect sensors, defined by Eq. 2:

$$threshold = noise_{channel}\sqrt{3n} \quad (2)$$

where n denotes the number of sensors on the PCB, with each sensor providing three-axis measurements, and $noise_{channel}$ is the 2-σ noise of Hall-effect sensor measurements from each axis in a static magnetic field. Eq. 2 applies a fair noise threshold that scales with the number of Hall-effect sensors. This ensures that ambiguity ratios are evaluated consistently across designs with different number of sensors.

4.1.2 Sensitivity to rotation. Sensitivity to rotation is defined as the change in sensor signal with respect to changes in the orientation of the magnetic ball. An ideal design maximizes this sensitivity. The sensitivity to rotation depends on the current pose, because the near-field magnetic field of multiple magnets create a complex magnetic field around it. Therefore, we picked a random and dense set of poses to reconstruct the distribution of rotational sensitivity.

As shown in Fig. 3(b), we randomly selected 1,000 circular paths. With 200 poses sampled along each path, we obtained sensor readings at 200,000 poses. Rotational sensitivity was then calculated as the derivative of the sensor array measurements with respect to the rotation angle (Eq. 3).

$$Sensitivity_{rotation} = \left\| \frac{d\vec{X}}{d\theta} \right\|_2 \quad (3)$$

where $\vec{X}$ is the sensor readings along a circular path and θ is the rotation angle. Fig. 3(b) bottom shows example sensor readings along a random circular path.

4.1.3 Sensitivity to force. Sensitivity to force is defined as the change in sensor signal with respect to compression from applied

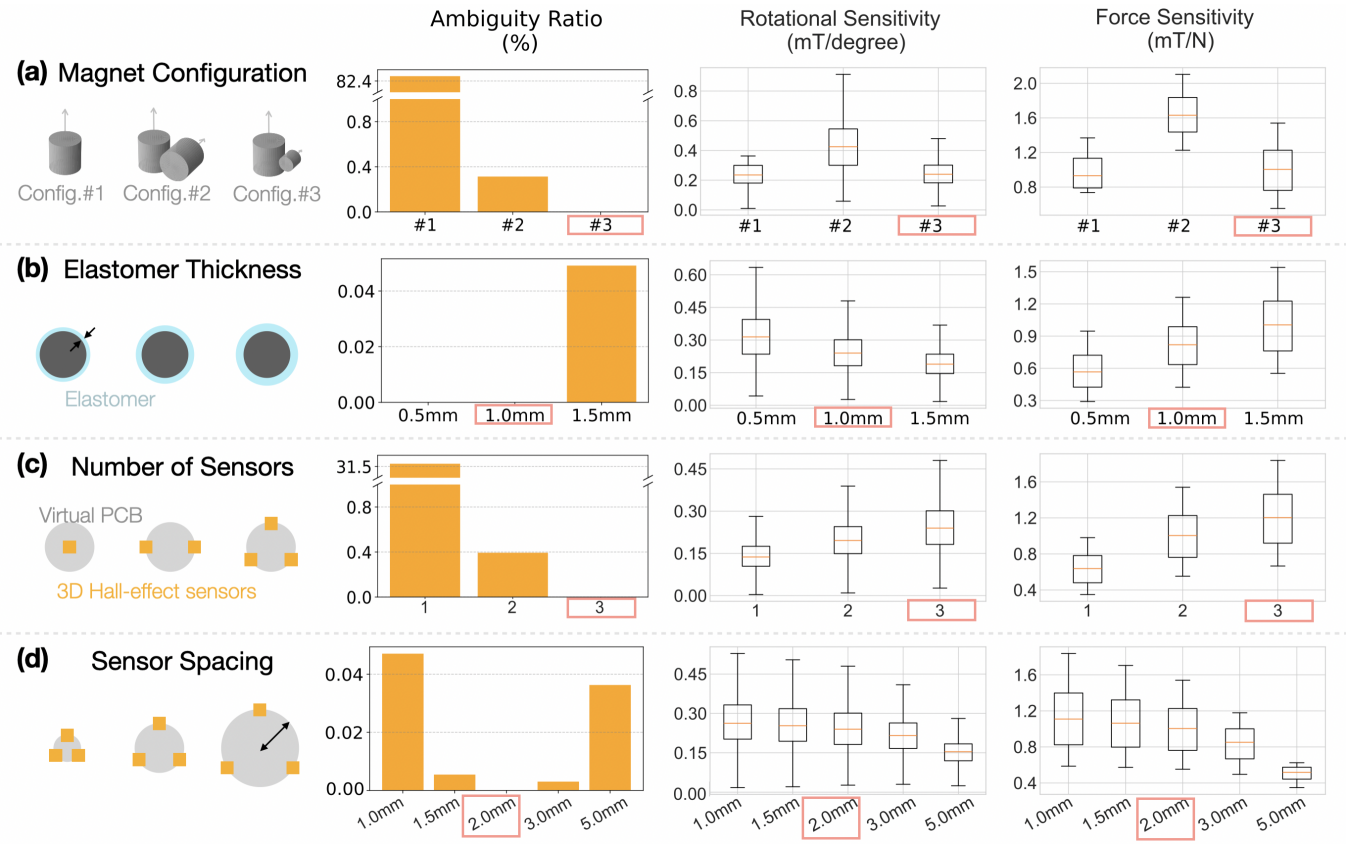

Figure 4: Ambiguity ratio, sensitivity to rotation, and sensitivity to forces for different designs in (a) magnet configuration, (b) elastomer thickness, (c) number of Hall-effect sensors and (d) spacing between the sensors.

force. We desire to maximize this sensitivity for accurate force sensing. Similar to rotational sensitivity, force sensitivity also depends on current pose. We sampled a 10,000 evenly distributed orientations, and applied compression up to 1 N. The sensitivity to force is calculated by Eq. 4.

$$Sensitivity_{force} = \left\| \frac{\Delta \vec{X}_{1N}}{\Delta F} \right\|_2 \tag{4}$$

where $\Delta \vec{X}_{1N}$ is the change in sensors signal between zero compression and 1 N compression and ΔF is the corresponding change in force. As shown in the bottom plot of Fig. 3 (c), the sensor signal changes nonlinearly with respect to force, which is a common behavior in soft force sensors [7, 12, 36]. Therefore, the linear slope from zero compression to 1 N is used as a representative sensitivity.

4.2 Sensor Designs

Through simulation, we optimize four key design parameters: magnet configuration, elastomer thickness, number of Hall-effect sensors, and sensor spacing (Fig. 4).

4.2.1 Magnet configuration. Magnet configuration refers to the geometrical arrangement of the embedded magnets, which was varied across three types of designs (Fig. 4 (a)). Config.#1 is a single cylindrical magnet; Config.#2 is two same-sized magnets oriented at right angles; Config.#3 is similar to Config.#2 but with two different-sized magnets. The choice of magnet configuration has a critical impact on the ambiguity ratio. As demonstrated in Fig. 4 (a), a single magnet (Config.#1) produces the most ambiguous measurements with over 80% of poses. Using two same-sized magnets (Config.#2) reduces ambiguity, but 0.2% of poses remains ambiguous. Config.#3, which employs two magnets of different sizes, eliminates all ambiguous poses, though at the cost of reduced sensitivity to rotation and force due to the smaller secondary magnet.

Ambiguity arises from two factors: symmetrical magnetic field and low signal-to-noise ratio. The magnetic field of a single magnet exhibits rotational symmetry due to its geometry and unidirectional polarization (Fig. 5(a)), meaning many poses along the symmetry axis yield identical sensor readings. The relatively low field strength further exacerbates the ambiguity, explaining the highest ambiguity ratio of Config.#1. A simple approach to break the symmetry is to introduce an additional magnet. However, the placement and properties of the second magnet must be carefully chosen to avoid introducing new symmetries. Two same-sized magnets in Config.#2 still exhibit point symmetry. As shown in Fig. 5(b), the magnetic field cross-sections for xy and zx planes are exactly the same, rotated by 90 degrees. This symmetry leads to identical sensor readings at

different poses, accounting for the remaining ambiguity despite the strongest field strength among the three. The remaining symmetries can be further eliminated by using a second magnet of different size (Fig. 5(c)). As a result, Config.#3 produces an asymmetric 3D magnetic field, yielding the lowest ambiguity ratio.

Overall, an asymmetric magnetic field with sufficient signal-to-noise ratio is necessary to minimize ambiguity, which is successfully achieved in Config.#3.

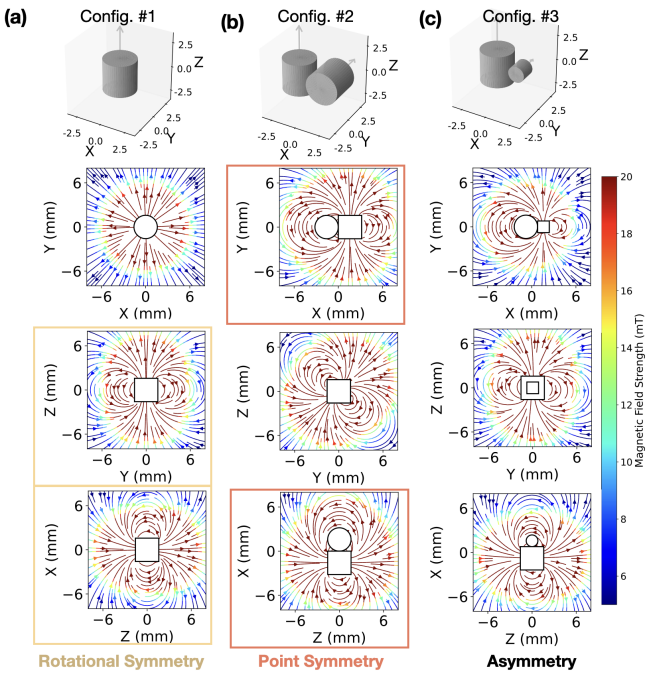

Figure 5: Simulated magnetic field cross-sections (xy, yz, zx planes) illustrating (a) rotational symmetry, (b) point symmetry, and (c) asymmetry.

4.2.2 Elastomer thickness. The elastomer thickness was adjusted between 0.5 mm and 1.5 mm (Fig. 4(b)). As the thickness of elastomer increases, ambiguity ratio and rotational sensitivity deteriorate, while force sensitivity exhibits the opposite trend (Fig. 4(b)). A thicker elastomer positions the sensors farther away from the magnet source, reducing the magnetic field strength and signal-to-noise ratio, which explains the higher ambiguity ratio and lower rotational sensitivity. In contrast, force sensitivity improves because the same force creates larger compression with thicker elastomer. Considering this trade-off, an elastomer thickness of 1.0 mm was chosen as a balanced design.

4.2.3 Number of sensors. We varied the number of Hall-effect sensors from one to three. For a single sensor, it was placed at the center of the virtual PCB. For multiple sensors, they were placed evenly along a circular arrangement on the PCB (Fig. 4(c)). Increase in number of sensors enhances all three evaluation metrics. However, fewer sensors are desired for compact sensor design. Estimating the pose of the MagBall involves six degrees of freedom (DoF): three rotational DoFs describing the ball's orientation (pitch, yaw, and roll) and three translational DoFs corresponding to compression along the x, y, and z axes. While two sensors theoretically suffice to resolve the six DoF (6 measurements and 6 unknowns), noise and limited sensor resolution necessitate additional redundancy. Ambiguity ratios indicate that three sensors are necessary to achieve robust pose estimation.

4.2.4 Spacing between sensors. Sensor spacing is defined as the radius of the circular arrangement, and it was varied from 1.0 mm to 5.0 mm (Fig. 4(d)). Sensor spacing has a non-monotonic effect on the ambiguity ratio while mean sensitivities to rotation and force decrease with increasing sensor spacing. Since the magnetic field around the ball varies spatially in strength and direction, distributed sensors are beneficial. For distributed sensors, if one sensor lies in a weak-field region, others are likely in stronger regions, stabilizing overall sensitivity. However, when sensors are tightly clustered, it is possible for all of them to fall in a weak-field region at certain poses, reducing robustness. This explains not only the initial decrease in ambiguity ratio but also the initial increase in the minima of rotational sensitivity. Beyond certain point, wider spacing increases ambiguity ratio reduces the minima of rotational sensitivity because the sensors are, on average, farther from the magnet source, leading to low signal strength and signal-to-noise ratio. The minima of force sensitivity did not exhibit the same trend, as it also depends on alignment with the radial compression direction, an effect that favors tightly spaced sensors. Based on this trade-off, spacing of 2.0 mm provided the most robust design with only little loss in rotational and force sensitivities.

In summary, our simulation results indicate that the following design parameters yield robust and sensitive sensor readings: two magnets of different sizes arranged at a right angle (Config. #3), an elastomer thickness of 1.0 mm, and three Hall-effect sensors arranged in a circle with a radius of 2.0 mm.

4.3 Implementation

Based on the insights from simulation, we implemented the MagBall prototype. The dimension of MagBall is 13 × 13 × 10 mm, small enough to be easily integrated into everyday objects. Moreover, the total price of one MagBall is less than 4.0 USD, which includes all components shown in Fig.6(a).

4.3.1 Fabrication. We fabricated the magnetic ball by 3D-printing (Formlabs Form 3) a rigid sphere with holes for two different-sized cylindrical N52 neodymium magnets (diameters and heights of 1.5875 mm, 3.175 mm). Then, magnets were inserted as Config.#3 in Fig.4(a). To cast a 1.0 mm elastomer layer (Vytaflex-30, Smooth-On), we used two molds: one with 1 mm supports to center the core and one without supports to produce a seamless surface. As a result, we fabricated a magnetic ball with diameter of 8 mm (Fig.6(b)).

The ball holder was also 3D-printed, and 1.5 mm stainless steel bearing balls (304, G100) were assembled into three bearing races. A bearing race is a ring-shaped track that allows the bearing balls to roll smoothly. Races were designed for free ball motion while retaining tightness with the magnetic ball. The ball holder was printed in two parts: the bottom to hold the magnetic ball and the top to secure it, preventing detachment (Fig.6(a)).

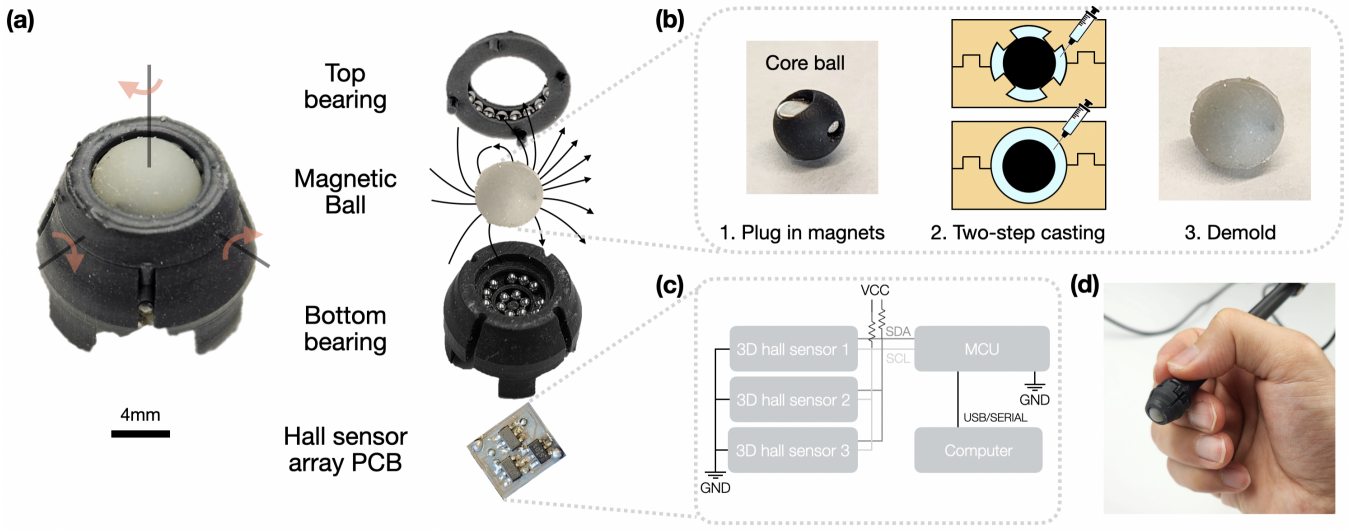

Figure 6: Fabrication of MagBall. (a) Assembly of MagBall. (b) Fabrication of the magnetic ball. (c) Circuit for I^2C communication between 3 Hall-effect sensors and MCU, connected to a computer for further estimation of displacement and force. (d) MagBall integrated into a stylus pen.

4.3.2 Circuit. We measure the 3D magnetic field using linear 3D Hall-effect sensors (TMAG5273, Texas Instruments). A custom PCB was designed with three sensor IC chips arranged in an equilateral triangle, such that their Hall-sensing elements lie on a circle with a 2.0 mm radius. Each sensor communicated with an MCU (Seeed Studio XIAO ESP32C3) via I^2C, and 9 measurements (3 axes magnetic field from 3 sensors) were sampled at 180 Hz (Fig.6(c)). Data were streamed to a computer in realtime.

4.3.3 Assembly. The complete assembly of MagBall is shown in Fig.6(a). At the base, the PCB with the Hall-effect sensor array is mounted beneath the bottom bearing. The magnetic ball rests on this bearing and is enclosed by a top bearing, forming the ball holder. Fig.6(d) illustrates our prototype integrated into a pen.

5 Results

We evaluate the performance of our MagBall prototypes and demonstrate its applications as a surface-independent stylus pen, wearable trackball ring and smart massage tool.

5.1 Experimental Validation

We evaluate the sensing performance of our prototype under rotation and force to validate the simulation results. We performed two separate experiments where the effects of rotation and applied force are decoupled. Both tests were performed with the magnetic ball without the elastomer layer, the core ball.

During the rotation test, the Hall-effect sensor array was fixed 7.5 mm from the core ball center, and the ball was rotated from five random initial orientations with our customized set-up (Fig.7 (a)). Rotation angles were measured with an encoder (AS5600). Using Magpylib, we simulated sensor array readings along the same five circular paths. The mean-squared-error between simulations and experiments was 0.972 mT. Fig.7(b) compares the sensor readings

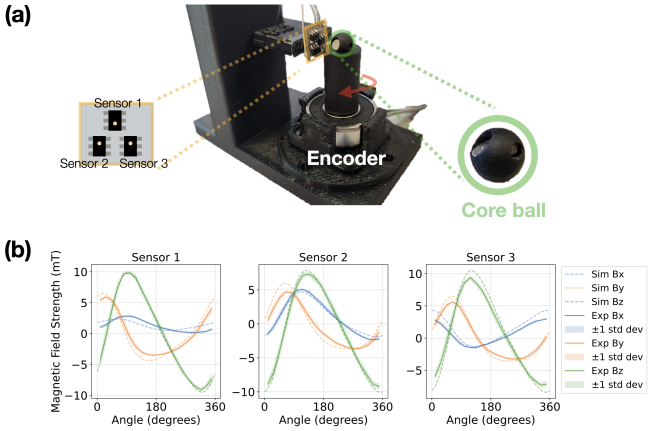

Figure 7: Experimental validation of sensor signal under rotation. (a) Experimental setup for sensor readings for rotation (b) Comparison between simulation and experimental magnetic field measurements with respect to rotated angle.

along one of the circular paths in the experiment and simulation. The discrepancies are attributed to experimental factors, including sensor misalignment during soldering, mismatch of initial ball orientation, and slight spin-axis precession. Because near-field magnetic fields are highly sensitive to small displacement, such errors likely accumulated to produce the observed gap between experimental and simulation results.

To validate sensing performance for forces, the Hall-effect sensor array was placed 7.5 mm below the ball center, separated by a 1 mm elastomer layer and 3D-printed part (Fig.8(a)). An Instron Universal Testing Machine compressed the ball from above at 1 mm/min up

to 0.5 mm (approximately 50% strain on elastomer), while displacement, compression force and Hall-effect sensor measurements were recorded. The tests were repeated at five random ball orientations. Simulations under same conditions yielded a mean squared error of 1.03 mT. Fig.8(b) shows a representative comparison. As with rotation, discrepancies are attributed to experimental factors.

Overall, the experimental results match the simulation predictions for both rotational and force sensing. Despite minor discrepancies caused by sensor misalignments, mismatch in initial ball orientations and very sensitive near-field magnetic field, the trends in magnetic field changes are consistent between simulation and experiment. These results validate that our simulation can reliably guide the design of MagBall for displacement and force estimation.

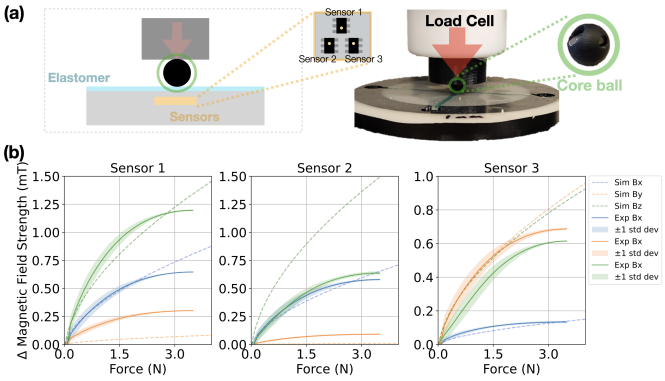

Figure 8: Experimental validation of sensor signal under force. (a) Experimental setup for Hall-effect sensor readings under applied force (b) Comparison between simulation and experimental magnetic field measurements with respect to applied compression force.

5.2 Estimation for Displacement and Force

Displacement and force information is inherently embedded in the change of magnetic field captured by the Hall-effect sensor array. Here, displacement refers to the two-dimensional movement of the contact point on the surface, resulting from the rotation of the magnetic ball. The near-field 3D magnetic field changes dynamically with spatial configuration. While this provides high sensitivity, it also makes the system vulnerable to fabrication mismatches, which can shift absolute sensor readings and sensitivities dramatically (Fig. 4, 7 and 8). To compensate for such variation in our manually fabricated prototype and ensure robust and accurate estimation, we adopted a data-driven approach. We estimate displacements and forces from the Hall-effect sensor signals via machine learning.

5.2.1 Data Acquisition. As our design is inspired by the tip of a ballpoint pen, we adopt a similar setup for scalable and accessible data acquisition. We integrated MagBall into the tip of a 3D-printed pen body (Fig. 6(d)), allowing users to perform writing tasks naturally while holding the pen.

In general, the data acquisition set-up consists of a transparent acrylic plate with a top-facing camera (Arducam B0385) at the bottom. The camera records the real-time contact position of the MagBall at the pen tip (Fig. 9(a)). The orientation of the pen was also tracked using markers (green circle, yellow square), enabling alignment of camera-based position data with the reference frame of PCB at the start of each sequence. Eight different shapes such as circles, rectangles and triangles were drawn in different sizes and speed for 30 seconds each. During drawing, the Hall-effect sensor array measurements were recorded at 180 Hz, and camera recorded the position at 100 Hz.

We implement a custom computer vision pipeline in OpenCV to obtain ground-truth trajectories of the pen tip and orientation markers. Three colored markers were detected in each frame based on color, size, shape, and displacement constraints relative to the previous frame. The resulting trajectories were resampled to 180 Hz to match the sampling rate of the sensors, and frames with occlusions were excluded. Fig. 9(b) shows some raw Hall-effect sensor array data corresponding to two camera-recorded trajectories used as ground-truth. In total, we captured 146,415 synchronized data points for displacement estimation.

To capture the force dataset, four load cells were mounted under an acrylic plate (Fig. 9(a)). The pen was pressed without rolling for five cycles at 550 random ball orientations. Similarly, the force data and Hall-effect sensor measurements were recorded at 180 Hz. We captured 223,850 data points for force estimation. Datasets for displacement and force estimation were collected separately. This setup helps minimize interference, as rolling induces vibrations that can perturb ground-truth force signal.

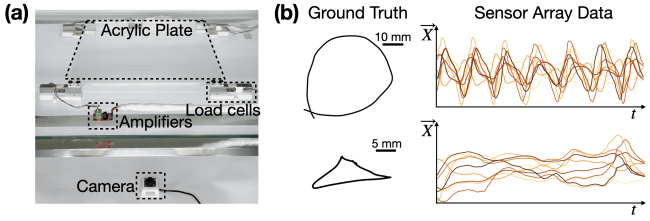

Figure 9: Data acquisition for machine learning models. (a) Experimental setup to obtain ground truth. A bottom camera captures the movement of MagBall on top of transparent acrylic plate supported by load cells. (b) Sample ground truth trajectories along with corresponding sensor array data.

5.2.2 Model. We test two machine learning models, Long Short-Term Memory (LSTM) [46] and ExtraTreesRegressor (ETR) [24], for displacement and force estimation. The LSTM network is lightweight with a single LSTM layer with hidden dimension of 64, followed by two fully connected layers with hidden dimensions of 64, which enable real-time inference. The ETR model, trained with 100 estimators and a minimum of 5 samples per leaf, also achieves fast, real-time predictions due to its tree structure.

To estimate displacement, we use 9-channel Hall-effect sensor readings and the inter-sample time as input. The model outputs per-sample displacement. Rather than predicting absolute position, the per-sample displacement prediction enables the generalization to canvases larger than the our data acquisition setup. For the force model, we extract 18 features from the 9-channel Hall-effect sensor

readings. The first 9 features are the channel-wise standard deviations. For each of the three magnetic field vector measurements, we computed the magnitudes, which were used to extract the remaining 9 features: mean over last 50 points (3 features), the deviation from this mean (3 features) and the first-order derivative (3 features). All inputs to both models were normalized. We randomly split the dataset into 80 % training and 20 % testing, ensuring that all data from a single source was assigned entirely to one set to prevent data leakage.

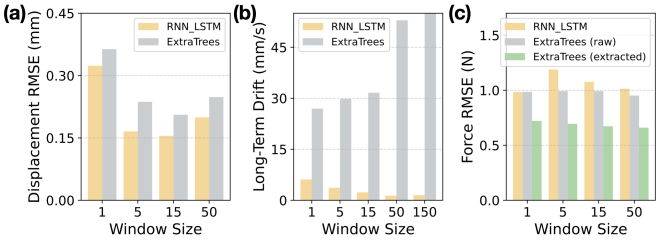

Figure 10: Effect of window size and model type on performance: (a) displacement estimation error, (b) long-term drift in position, and (c) force estimation error.

5.2.3 Results. Fig.10 presents the effect of window size on estimation accuracy and long-term drift. Displacement inference achieves the lowest error with the LSTM model at a window size of 15, while long-term drift is lowest at a window size of 50. The long-term drifts are computed as the slope of a linear fit to the positional error over time in the test dataset, with estimated positions obtained by cumulatively summing the predicted displacements. For force inference, ETR with extracted features performs best at a window size of 50. In terms of both short-term and long-term errors for displacement, the temporal pattern of the signal improves displacement estimation, but large window sizes begin to introduce less relevant data, leading to increased error. The difference in optimal window sizes arises because larger windows could apply smoothing, which would slightly increase short-term error by blurring rapid changes. For force estimation, models perform poorly when using raw Hall-effect sensor data. With the extracted features, the accuracy of the ETR model improves as the window size increases and plateaus once it reaches 15. Therefore, we adopt the LSTM (window size 15) for displacement and the ETR with extracted features (window size 15) for force. On the test dataset, our models have RMSE of 0.15 mm and long-term drift of 2.31 mm/s for displacement, and RMSE of 0.67 N for force. Fig.11 illustrates sample trajectories obtained by cumulatively summing predicted displacements. Predicted paths closely match the overlaid ground truth across different scales of drawings. The inference from the models take 4.9 ms in total, which is sufficient for real-time rendering of the contact interaction.

Overall, MagBall reliably estimates displacement and force. In particular, displacement inference achieves sub-millimeter precision, enabling high-precision applications such as stylus pens, wearable trackball, and massage monitoring.

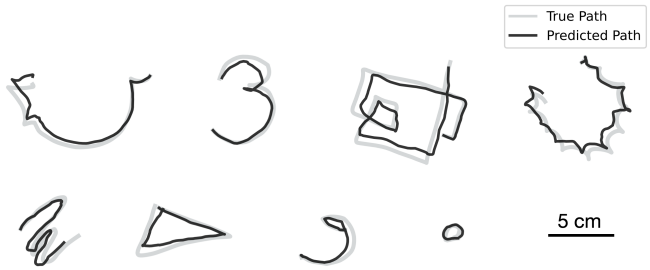

Figure 11: Example path tracking results by cumulative summation of estimated displacements, overlaid with ground truth from camera.

5.3 Compatibility with Diverse Surfaces

The rolling mechanism of MagBall enables operation across a wide range of real-world surfaces. In the previous section, the machine-learning models were trained and tested using interaction data collected on an acrylic surface that is chosen solely because of its transparency that allows accurate ground-truth capture through camera recording. The same models generalize to a wide variety of other surfaces. Although surfaces vary widely in geometry and material properties, we broadly categorize them along three dimensions: flat vs. non-flat, rigid vs. soft, and magnetic vs. non-magnetic. We evaluate MagBall on six surfaces that collectively cover these dimensions.

To obtain ground-truth for contact position, we attached a marker parallel to the MagBall pen (Fig. 12(a)). During drawing, the marker produced a visible trace on the surface, which was used as the ground-truth contact path in our analysis (Fig. 12(b)). We note that this approach introduces small but unavoidable errors due to slight yaw rotation and differences in how the two tips contact the surface. Then, four shapes (circle, star, square and scribble) are drawn, ranging from 30 mm to 70 mm in size, on six different surfaces (cardboard, glass, water bottle, cushion, magnetic sheet and metal locker) with the MagBall pen and marker in parallel (Fig. 13(a)). The drawings on the water bottle were smaller with sizes ranging from 15 to 50 mm, for it was difficult to maintain the two point contacts on the curved surface with radius of curvature of approximately 4.5 cm. A moving average filter with a window size of 25 was applied to smooth the MagBall-computed path.

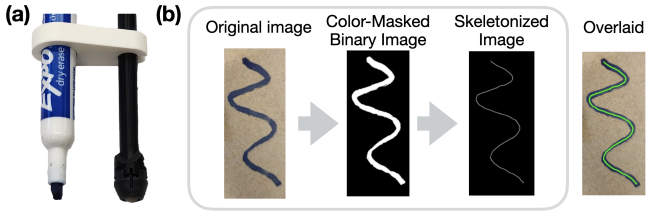

Figure 12: Ground-truth path acquisition using marker tracing. (a) A marker and a MagBall pen connected in parallel to obtain ground-truth data. (b) Marker path extracted via color masking and skeletonization.

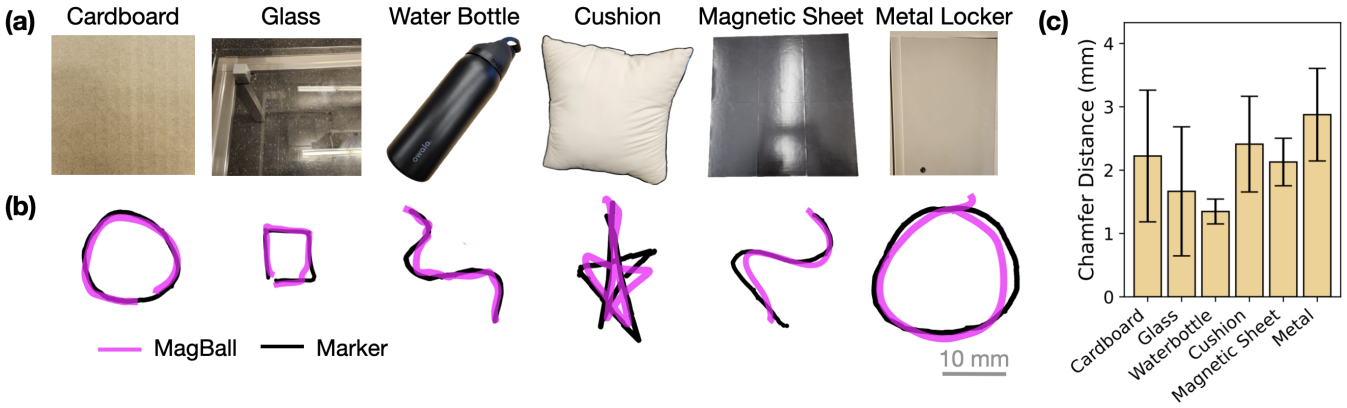

Figure 13: Compatibility with diverse surfaces. (a) The six surfaces evaluated: cardboard, glass table, water bottle, cushion, magnetic sheet and metal locker. (b) Sample drawings from marker and MagBall for each surface. (c) Chamfer distance of drawings from the marker and MagBall for different surfaces.

We evaluate the accuracy of MagBall by Chamfer distance, because there is no one-to-one correspondence between the points on marker-path and MagBall-computed path. Chamfer distance is defined by Eq. 5:

$$CD(P,Q) = \sqrt{\frac{1}{2|P|}\sum_{p\in P}\min_{q\in Q}\|p-q\|_2^2 + \frac{1}{2|Q|}\sum_{q\in Q}\min_{p\in P}\|q-p\|_2^2} \tag{5}$$

where P is the set of MagBall-computed 2D points with cardinality $|P|$, Q is the marker-based ground-truth 2D point set with cardinality $|Q|$, and p and q are the 2D position vectors of a point in the set P and Q. The Chamfer distance measures the mean deviation between two paths. It penalizes both when the MagBall-computed points are far away from ground-truth path and when the MagBall-computed points fail to cover some parts of the ground-truth path. Lower Chamfer distance, therefore, indicates higher similarity between drawings. As shown in Fig. 12(b), the 2D path coordinates of marker drawing was obtained by extracting the centerline of the marker drawing through color masking followed by skeletonization.

MagBall operates consistently across six different surfaces. Fig. 13(b) shows some examples of the ground-truth marker drawings overlaid with MagBall-computed paths. The Chamfer distance between marker and MagBall drawings agree with each other within the error margins across surfaces (Fig. 13(c)). Notably, the metal locker and magnetic sheet were magnetic. The magnetic ball from our sensor could even stick to the metal surface, if disassembled from the holder. Despite the magnetic interference, position tracking performance was unaffected. The Hall-effect sensor array, positioned roughly 10 mm away from the contacting surface, experiences negligible distortion in the magnetic field from the metal or magnetic sheet, allowing reliable measurements.

5.4 User Study

We conducted a user study to investigate user experience and usability of Magball across different surfaces under which conventional input devices cannot operate. This study was approved by our institution's Institutional Review Board (IRB).

5.4.1 Procedure. Eight participants (3 female, 5 male; age = 24 ± 3) performed a same task with a MagBall pen or commercial devices: a stylus pen (Intuos Small, Wacom), mouse (M340, Logitech), and trackpad (Macbook Pro, Apple). These commercial devices, which are highly optimized for their specific operating environment, provide a useful upper-bound reference for MagBall's performance.

After a brief introduction to MagBall's operation, participants were asked to follow a bird-shaped line template on a computer screen using the MagBall pen or commercial input devices (Fig. 14(a,c)). The system rendered user's input in real time on top of the template. Although the template itself consisted of a single continuous line, participants completed it through multiple strokes, with each new stroke starting at the endpoint of the previous one. Before the actual trials, participants were allowed to practice on four different surfaces: an acrylic plate, a magnetic sheet, a pillow, and the thigh area of their own pants. The pants surfaces varied widely, including jeans, cotton pants, corduroy pants, sweatpants and athletic pants. In total, each participant completed seven drawings of the same bird template: four using the MagBall pen on four different surfaces and three using the three commercial input devices. The order of seven drawing conditions was randomized across participants, and all drawing paths were recorded for analysis.

5.4.2 Results. Fig. 14(c,d) shows example drawings from each of the seven conditions by one participant. In general, all users were able to follow the template. Chamfer distance (Eq. 5) between the drawn path and ideal template were calculated (Fig. 14(e)). Drawings produced with MagBall showed a comparable mean Chamfer distance to those obtained with the three commercial input devices. However, the variance was noticeably higher in all four MagBall surface conditions. Additionally, we calculated the completion time of each drawing, and users reported difficulty of drawing on the seven conditions on a 1-7 scale. Both completion time and difficulty were higher for MagBall compared to commercial devices, as shown in Fig. 14(f,g), because participants were less familiar with MagBall and required more time to control it effectively. Several participants reported that MagBall felt smoother on soft surfaces: pillow and pants. This may have caused slightly larger mean completion time

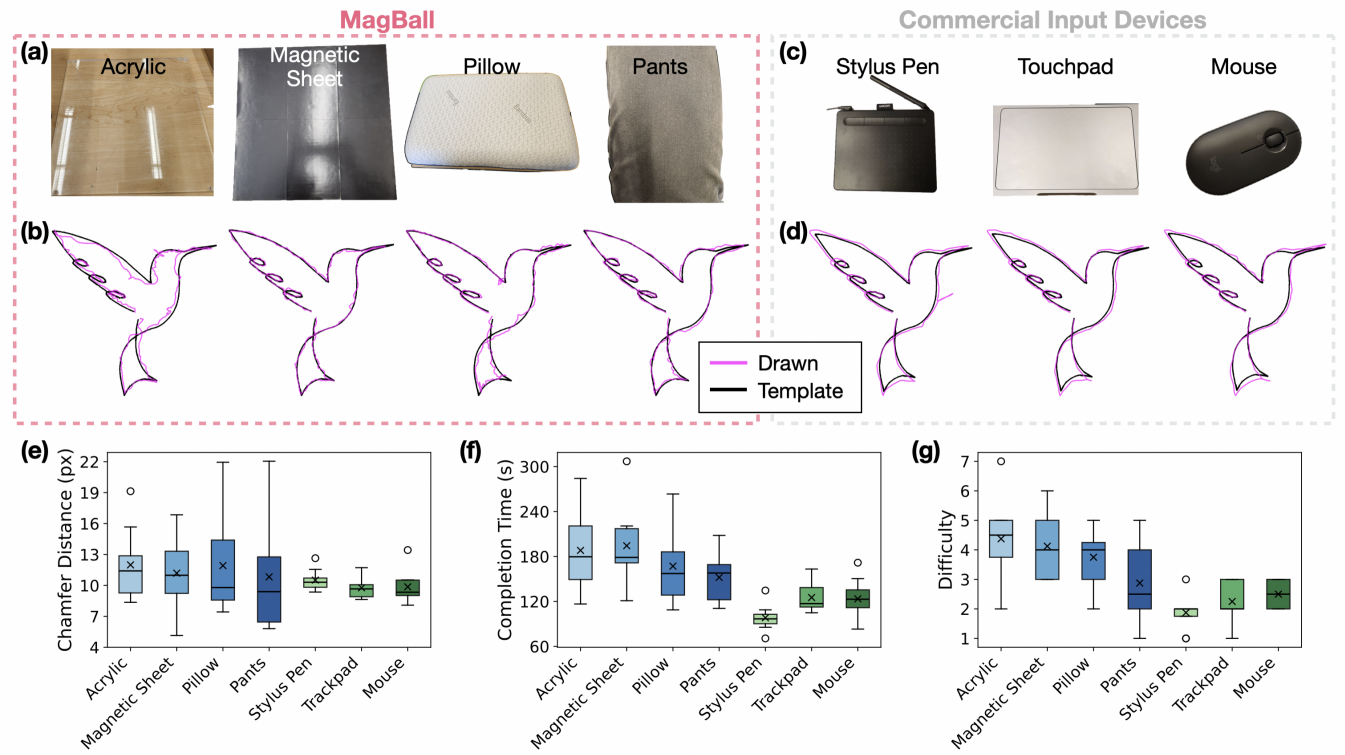

Figure 14: User study to compare MagBall pen with commercial input devices. (a) Four drawing surfaces for the MagBall pen: acrylic, magnetic sheet, pillow and pants. (c) Three commercial input devices used for the same task: stylus pen, trackpad and computer mouse. (b,d) Sample drawings from each condition by one participant. (e) Chamfer distance between user's drawing and template. (f) Task completion time. (g) Difficulty reported by participants. For box plots, left four blue plots are for MagBall on different surfaces, and right three green plots are from three commercial input devices. The circles in box plots indicate outliers beyond 1.5× the interquartile range (IQR).

and difficulty rating for the two rigid surfaces compared to the soft ones. We attribute this to the unevenness in the fabricated magnetic ball. Due to abrasion and limited precision in 3D-printing and casting, the diameter of magnetic ball varied between 7.2 mm and 7.9 mm after data collection, various experiments and user study. This uneven geometry was less noticeable on soft surfaces, which deform to accommodate the shape, but was more prominent on rigid ones, making it feel bumpy. Refinement on fabrication will improve the smoothness of the rolling, enhancing overall performance and reducing variance in performance among different surfaces.

From the post-session interview, six participants reported that they did not perceive any delay between their hand movement and the displayed stroke, while two participant reported perceiving a slight delay comparable to that of commercial tablets. In addition, the rolling of the ball could provide a pleasant tactile experience, as a participant commented that "[he/she] really liked feeling the rotation process of the pen as it offers really good tactile feedback."

Although performance metrics of MagBall are slightly worse than those of commercial devices, MagBall is not intended as a direct replacement. Instead, it extends the precise contact-based interaction into far less constrained environments. Participants envisioned several usage scenarios that are either infeasible or poorly supported with conventional input devices: 1) drawing diagrams on one's pants when an idea struck, 2) tracing the contours of objects to capture shapes or dimensions, 3) sketching in a confined space such as trains or airplanes with AR/VR devices as portable screens.

With its capability to sense sliding-contact interactions and its broad compatibility with real-world surfaces, MagBall holds significant potential for a range of applications.

6 Applications

We demonstrate applications of our sensor to measure precise displacement and force in a surface-independent stylus pen, wearable trackball ring and smart massage tool.

6.1 Surface-Independent Stylus Pen

The integration of our system as an interactive pen is a natural and compelling use case. By replacing the pen's ball tip with MagBall, we could digitize contact interactions between the pen and arbitrary surfaces. These rich multimodal signals can then be used as surface-independent input for digital systems. Unlike commercial stylus pens, our design does not require active surfaces such as touchscreens, reducing the need for bulky surface-devices to help digitize writing and drawing.

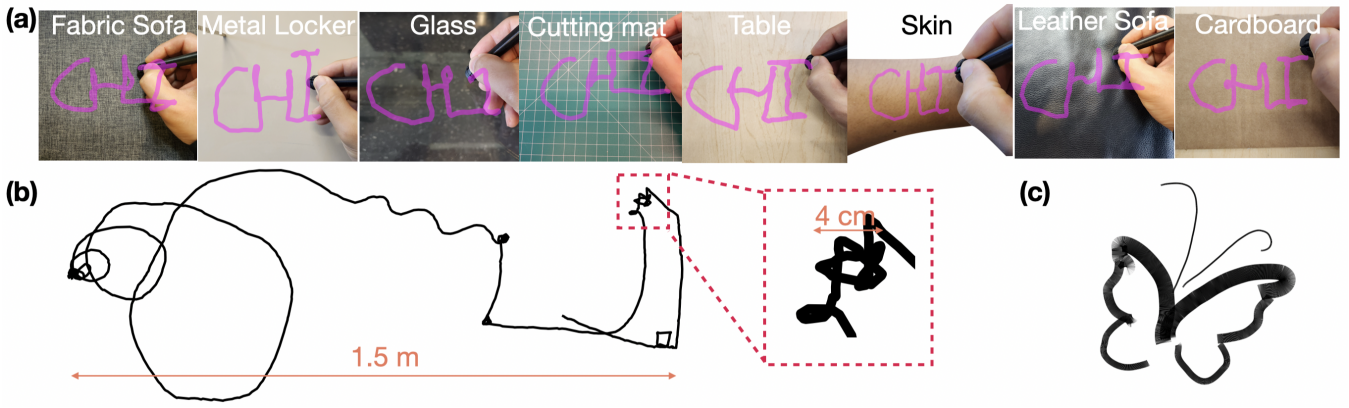

Figure 15: Surface-independent stylus pen. (a) The MagBall pen works on a variety of surfaces, including magnetic metal, transparent glass, soft sofa material and human skin. (b) It enables drawings of multiple scales from centimeters to meters. (c) A drawing of a butterfly by MagBall pen with four different stroke widths adjusted by its force measurements.

Fig.15(a) illustrates the surface independence of our pen. "CHI" was written on various surfaces, including a fabric sofa, leather sofa, cutting mat, table, metal locker, cardboard, glass and human skin. Because all sensing occurs within the pen, no additional instrumentation was needed on any of those surfaces. MagBall relies on no-slip rotation to translate user interaction into measurable signals. With the high friction of elastomers with most materials [44], MagBall is compatible with diverse passive surfaces.

Although the interaction is based on point-contact, the rolling mechanism enables multi-scale spatial interaction (Fig.15(b)). While the entire drawing is in meter-scale, centimeter-scale features exist within the drawing, which requires millimeter-scale precision. In order to achieve such high spatial resolution over large surface area, conventional sensing-grid approaches require compact electrode placement over the entire sensing surface. Furthermore, MagBall's force-sensing can be leveraged to modulate drawing parameters for nuanced drawing. A butterfly was drawn with four distinct stroke widths by modulating contact force with real-time on-screen rendering (Fig.15(c)). Our pen is a compact, portable and self-contained solution that allows multi-scale drawing on diverse surfaces.

6.2 Wearable Trackball Ring

Our fingertip offers high tactile spatial sensitivity, discriminating contact points just 1–2 mm apart [25]. To fully take advantage of this natural acuity, an input device must detect movement at a comparable scale. MagBall can function as a highly precise wearable trackball that captures micro-movements at the fingertip as input.

Fig.16(a) shows our wearable trackball mounted on an index finger. A thumb can manipulate the trackball with minute gestures to control a user interface. In our demonstration, estimated displacements from MagBall directly controlled the mouse cursor on a computer screen. As shown in Fig.16(b), the user adjusted the view angle of a 3D model into three angles using the wearable trackball in a Computer-Aided Design (CAD) program (Fusion 360, Autodesk). The displacement lengths between the three poses were only 6.1 mm and 9.0 mm, highlighting the fine-grained interactions between the user and our wearable trackball ring.

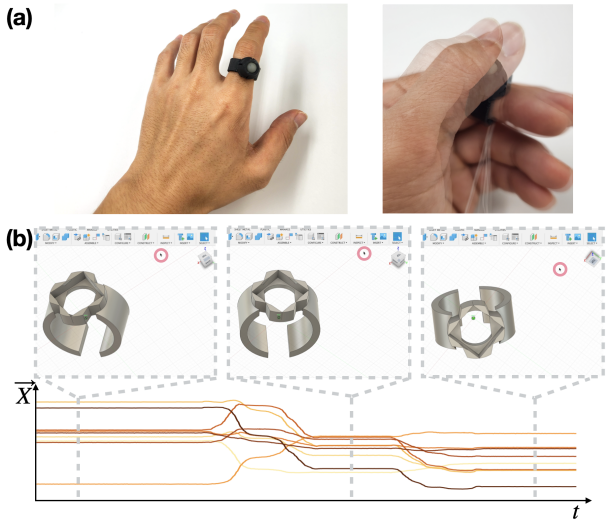

Figure 16: Wearable trackball ring. (a) The MagBall ring worn on the index finger can be easily manipulated by the thumb. (b) MagBall-computed displacements control cursor movements, enabling precise 3D view adjustments in a CAD program. The red circles indicate the mouse cursor positions.

6.3 Smart Massage Tool

With its compatibility with diverse surfaces and smooth rolling motion, MagBall is well-suited for integration into massage tools (Fig.17(a)). Our smart massage tool can evaluate massage motion in real time, helping to prevent ligament injury and support effective recovery [8]. During the warm-up phase, it measures massage speed (Fig.17(b)), enabling users to adjust their pace for safer preparation. In the subsequent phase, it tracks displacement to monitor massage position and guide users toward documented trigger-point locations (e.g., six in the anterior forearm, Fig.17(c)). Our massage

tool also monitors applied pressure and duration, ensuring users to effectively relieve tension at trigger-points.

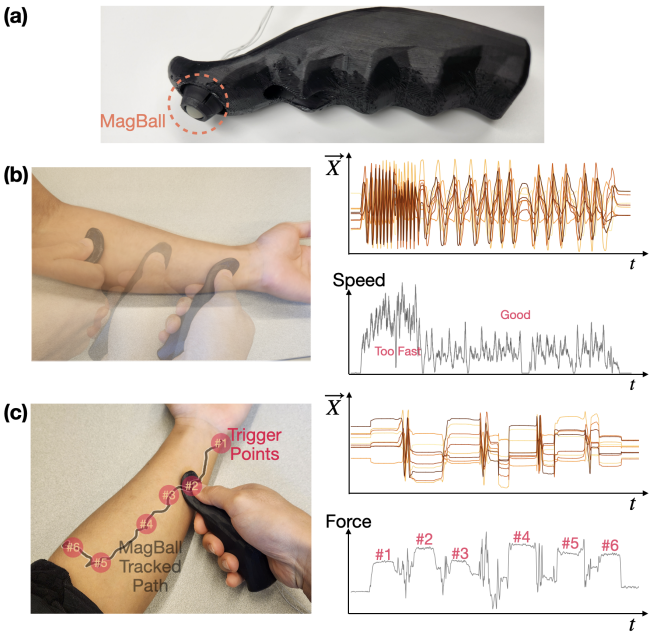

Figure 17: Smart massage monitoring tool. (a) MagBall integrated into a massaging tool. (b) The tool monitors massage speed to ensure a safe warm-up phase. (c) It guides users to target trigger points with appropriate force and duration for effective massage.

7 Discussion

We introduce MagBall, a magnetic-ball sensing system that captures linear displacement, motion direction, and applied force through the rotation of a magnet-embedded ball over an array of Hall-effect sensors. The design is compact, compatible with diverse objects, and capable of capturing a wide range of interactions. Although the system demonstrates promising results, some technical limitations remain to fully realize its scalability and performance.

7.1 Limitations

Failure under strong magnetic interference. While MagBall is compatible with most everyday surfaces, the system can fail under strong magnetic interference. As shown in earlier sections, it operates robustly on ordinary magnetic surfaces such as metal plates or weak magnetic sheets. This robustness arises because the 3D Hall-effect sensors are positioned more than 10 mm above the contact surface. For instance, the magnetic field of the magnetic sheet was approximately 6 mT at 1 mm above the surface, but it was less than 0.1 mT at a height of 10 mm. The rapid decay of magnetic field with distance ensures that the sensor measurements are minimally affected by weak or moderate magnetic sources commonly encountered in daily environments.

However, strong permanent magnets such as Neodymium magnets are able to distort the sensor readings to affect the estimation accuracy. To illustrate this limitation, we conducted a simple experiment in which we drew multiple straight lines with the MagBall pen near a cubic N52 magnet (Fig. 18). The magnet remained stationary, and each line corresponded to a different separation from the magnetic source, producing different levels of magnetic interference. It may be noted that the interference magnitude is not constant along each line. The value shown next to each line in Fig. 18 represents the maximum interference magnitude encountered along that stroke. MagBall remained functional under mild interference but failed once the magnetic field exceeded approximately 0.4 mT. Although this demonstration does not provide an exact failure threshold, it clearly shows that MagBall withstands moderate magnetic disturbances yet fails under strong magnetic interference.

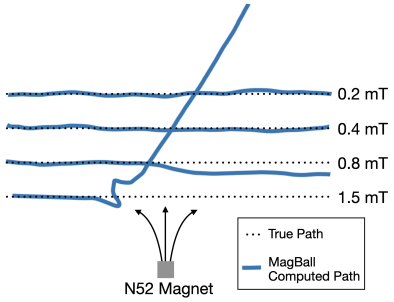

Figure 18: MagBall under different levels of magnetic interference.

Long-term drift of computed contact position. MagBall exhibits inherent drift in its position estimates due to the cumulative integration of predicted displacements. This behavior is unavoidable, as MagBall operates without any instrumented surface capable of providing absolute position references, unlike commercial tablets. In our user study, participants were able to compensate for long-term drift using visual feedback. As shown in Fig. 19, the deviation from the ideal template increases temporarily but returns toward zero rather than growing unbounded during 150-second drawing. This pattern indicates that participants corrected their drawing motion as they monitored the real-time rendering.

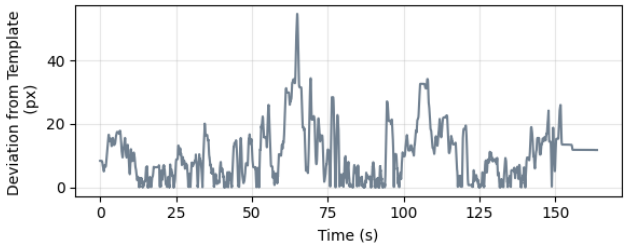

Figure 19: Deviation of the MagBall-drawn line from template over time. This data corresponds to the drawing on the pillow in Fig. 14(b).

Critical role of yaw in displacement estimation. It is imperative to compensate for yaw rotation in a single-body sensing system such as MagBall and prior optical-flow approaches [9, 37, 48], to accurately compute displacement or position in the world reference frame. Fig. 20 illustrates two simple scenarios demonstrating how yaw rotation affects the reconstructed path when compensation is absent. In Fig. 20(a), the device rotates by 90 degrees in yaw between two straight strokes. Because the pen undergoes the same downward motion in both strokes, failing to account for yaw results in a single straight segment instead of two perpendicular line segments. Such yaw changes can occur continuously within a single stroke. In Fig. 20(b), the device traces a quarter-circle path with simultaneous yaw rotation. From the pen's local reference frame, it experiences only tangential motion, which always points to the right. Consequently, the trajectory reconstructed without yaw compensation becomes a straight rightward line, instead of the quarter-circle. In MagBall, the raw magnetic field signal is designed to contain yaw information. The machine-learning model therefore learns to compensate for yaw rotation from data, so it outputs displacement in the correct world reference frame. However, it cannot resolve yaw rotation during off contact. During the user study, we observed that some participants were confused with orientation when they unintentionally rotated the MagBall pen in yaw direction during off-contact. Additional sensors such as inertial measurement units are required to compensate for off-contact yaw rotation.

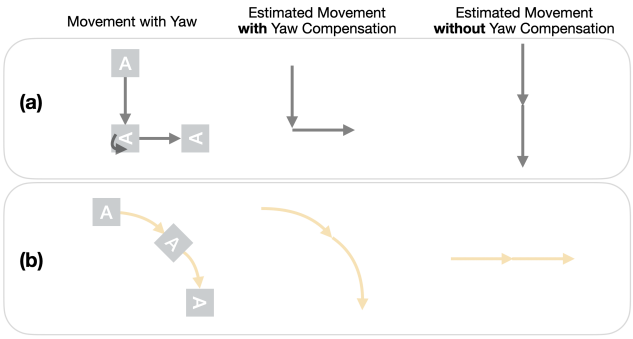

Figure 20: Incorrect estimation of movement without yaw compensation. (a) Example scenario with isolated yaw motion from a top view. "A" shows the yaw orientation of the device at different moments during the movement. (b) Example scenario with simultaneous yaw and displacement.

7.2 Future Works

Inertial measurement units implementation. MagBall is currently not able to track off-contact motions, because sensing mechanism requires rotation of the ball with contacting surface, which then changes the magnetic field measurements. When there is no contact, the ball would not spin, leading to no change in signal. This could hamper natural writing and drawing experiences where users usually hover the pen slightly between different strokes. Integrating inertial measurement units into MagBall could provide additional information about off-contact displacements, ensuring continuous tracking during brief off-contact.

MagBall array for robotic skin. While MagBall is currently a single point-contact device, extending it to an array could enable multi-point interaction measurements. In robotics, such arrays could provide tactile information for sliding contact events, which are ubiquitous in both daily life and manipulation tasks. Moreover, applying customized magnetic fields, we could use MagBall arrays as variable frictional interfaces. This enables integration of both sensing and actuation at robotic fingertips in a compact design.

Computational design of MagBall. The development of a computational design pipeline would further allow systematic optimization of MagBall's geometry, elastomer and magnet configuration, thereby facilitating rapid customization for diverse application requirements. Depending on applications, users may require higher displacement resolution or wider force range. Especially, adjusting the ball size, magnet sizes or varying the elastomer composition would permit tuning across a wide spectrum of force ranges, from subtle brushing to whole-body pressure input.

Wireless communication. To improve MagBall's portability and broaden its deployment scenarios, the sensing module can be equipped with an onboard battery and a compact wireless module. Integrating low-power technologies such as Bluetooth Low Energy would enable connectivity to nearby computing platforms, including smartwatches, smartphones, and AR glasses. This will support more convenient and natural interaction workflows.

8 Conclusion

In summary, MagBall provides a compact, robust, and versatile sensing platform that bridges the gap between point-contact devices (e.g., joysticks, buttons) and surface-based systems (e.g., touchpads). Our work identifies key design considerations and presents approaches to improve robustness and sensitivities. We implemented a prototype of MagBall that reliably estimates the displacement and applied force with data-driven approach. We also present practical applications including a surface-independent stylus pen, wearable trackball ring and smart massage tool. By combining the familiar rollerball with magnetic sensing, this work introduces a new type of interaction device and points toward future studies that exploit rolling mechanism for unbounded spatial interaction.

Acknowledgments

This work was supported by UW Royalty Research Fund, and UW ECE postdoc entrepreneurship fellowship.

References

[1] Anoto. 2025. Anoto Website. https://www.anoto.com/.
[2] Peter Berkelman, Bernadette Tix, and Hamza Abdul-Ghani. 2019. Electromagnetic Position Sensing and Force Feedback for a Magnetic Stylus With an Interactive Display. *IEEE Magnetics Letters* 10 (2019), 1–5. https://doi.org/10.1109/LMAG.2018.2886339
[3] bigclivedotcom. 2019. Inside a vintage PC gameport analogue trackball. https://www.youtube.com/watch?v=05t6VXcTy98.
[4] bigclivedotcom. 2024. inside an optical trackball. https://www.youtube.com/watch?v=aA0e2Rnjy8g&t.
[5] Yanling Bu, Lei Xie, Yafeng Yin, Chuyu Wang, Jingyi Ning, Jiannong Cao, and Sanglu Lu. 2021. Handwriting-assistant: Reconstructing continuous strokes with millimeter-level accuracy via attachable inertial sensors. *Proceedings of the ACM on Interactive, Mobile, Wearable and Ubiquitous Technologies* 5, 4 (2021), 1–25.
[6] Justin Chan and Shyamnath Gollakota. 2017. Data Storage and Interaction using Magnetized Fabric. In *Proceedings of the 30th Annual ACM Symposium on*

User Interface Software and Technology (Québec City, QC, Canada) *(UIST '17)*. Association for Computing Machinery, New York, NY, USA, 655–663. https://doi.org/10.1145/3126594.3126620

[7] Jungrak Choi, Donguk Kwon, Kyuyoung Kim, Jaeho Park, Dionisio Del Orbe, Jimin Gu, Junseong Ahn, Incheol Cho, Yongrok Jeong, Yongsuk Oh, et al. 2019. Synergetic effect of porous elastomer and percolation of carbon nanotube filler toward high performance capacitive pressure sensors. *ACS applied materials & interfaces* 12, 1 (2019), 1698–1706.

[8] E. Ernst. 2003. The safety of massage therapy. *Rheumatology* 42, 9 (sep 2003), 1101–1106. https://doi.org/10.1093/rheumatology/keg306

[9] Andreas Fender and Mohamed Kari. 2024. OptiBasePen: Mobile Base+ Pen Input on Passive Surfaces by Sensing Relative Base Motion Plus Close-Range Pen Position. In *Proceedings of the 37th Annual ACM Symposium on User Interface Software and Technology*. 1–9.

[10] Kenneth P. Fishkin. 2004. A taxonomy for and analysis of tangible interfaces. *Personal Ubiquitous Comput.* 8, 5 (Sept. 2004), 347–358.

[11] Alex M. Grau, Charles Hendee, John-Ross Rizzo, and Ken Perlin. 2014. Mechanical force redistribution: enabling seamless, large-format, high-accuracy surface interaction. In *Proceedings of the SIGCHI Conference on Human Factors in Computing Systems* (Toronto, Ontario, Canada) *(CHI '14)*. Association for Computing Machinery, New York, NY, USA, 4137–4146. https://doi.org/10.1145/2556288.2557172

[12] Chankyu Han, Jungrak Choi, Junseong Ahn, Hyunjin Kim, Ji-Hwan Ha, Hyeonseok Han, Seokjoo Cho, Yongrok Jeong, Jimin Gu, and Inkyu Park. 2023. Spike-based Self-Calibration for Enhanced Accuracy in Self-powered Pressure Sensing. *Advanced Materials Technologies* 8, 19 (2023), 2301199.

[13] Changyo Han, Ryo Takahashi, Yuchi Yahagi, and Takeshi Naemura. 2020. PneuModule: Using Inflatable Pin Arrays for Reconfigurable Physical Controls on Pressure-Sensitive Touch Surfaces. In *Proceedings of the 2020 CHI Conference on Human Factors in Computing Systems* (Honolulu, HI, USA) *(CHI '20)*. Association for Computing Machinery, New York, NY, USA, 1–14. https://doi.org/10.1145/3313831.3376838

[14] Ken Hinckley. 2002. *Input technologies and techniques*. L. Erlbaum Associates Inc., USA, 151–168.

[15] Hao Hu, Chengqian Zhang, Chengfeng Pan, Huangzhe Dai, Haonan Sun, Yifeng Pan, Xinyi Lai, Chenxin Lyu, Daofan Tang, Jianzhong Fu, and Peng Zhao. 2022. Wireless Flexible Magnetic Tactile Sensor with Super-Resolution in Large-Areas. *ACS Nano* 16, 11 (Nov. 2022), 19271–19280. https://doi.org/10.1021/acsnano.2c08664

[16] Jiawei Huang, Tsuyoshi Mori, Kazuki Takashima, Shuichiro Hashi, and Yoshifumi Kitamura. 2015. IM6D: Magnetic tracking system with 6-DOF passive markers for dexterous 3D interaction and motion. *ACM Transactions on Graphics (TOG)* 34, 6 (2015), 1–10.

[17] Kunpeng Huang, Yasha Iravantchi, and Alanson P. Sample. 2025. MagDeck: Surface-Based Object Recognition and Tracking via Passive Magnetic Sensing. In *Proceedings of the Extended Abstracts of the CHI Conference on Human Factors in Computing Systems (CHI EA '25)*. Association for Computing Machinery, New York, NY, USA, Article 385, 7 pages. https://doi.org/10.1145/3706599.3719882

[18] Sungjae Hwang, Myungwook Ahn, and Kwang-yun Wohn. 2013. MagGetz: customizable passive tangible controllers on and around conventional mobile devices. In *Proceedings of the 26th Annual ACM Symposium on User Interface Software and Technology* (St. Andrews, Scotland, United Kingdom) *(UIST '13)*. Association for Computing Machinery, New York, NY, USA, 411–416. https://doi.org/10.1145/2501988.2501991

[19] Sungjae Hwang, Andrea Bianchi, Myungwook Ahn, and Kwangyun Wohn. 2013. MagPen: magnetically driven pen interactions on and around conventional smartphones. In *Proceedings of the 15th International Conference on Human-Computer Interaction with Mobile Devices and Services* (Munich, Germany) *(MobileHCI '13)*. Association for Computing Machinery, New York, NY, USA, 412–415. https://doi.org/10.1145/2493190.2493194

[20] Kai Kuikkaniemi, Vilma Lehtinen, Matti Nelimarkka, Max Vilkki, Jouni Ojala, and Giulio Jacucci. 2014. Designing for presenters at public walk-up-and-use displays. In *Proceedings of the 8th International Conference on Tangible, Embedded and Embodied Interaction* (Munich, Germany) *(TEI '14)*. Association for Computing Machinery, New York, NY, USA, 225–232. https://doi.org/10.1145/2540930.2540949

[21] Kai Kuikkaniemi, Max Vilkki, Jouni Ojala, Matti Nelimarkka, and Giulio Jacucci. 2013. Introducing Kupla UI: a generic interactive wall user interface based on physics modeled spherical content widgets. In *Proceedings of the 2013 ACM International Conference on Interactive Tabletops and Surfaces* (St. Andrews, Scotland, United Kingdom) *(ITS '13)*. Association for Computing Machinery, New York, NY, USA, 301–304. https://doi.org/10.1145/2512349.2514588

[22] Han-Chih Kuo, Rong-Hao Liang, Long-Fei Lin, and Bing-Yu Chen. 2016. GaussMarbles: Spherical Magnetic Tangibles for Interacting with Portable Physical Constraints. In *Proceedings of the 2016 CHI Conference on Human Factors in Computing Systems* (San Jose, California, USA) *(CHI '16)*. Association for Computing Machinery, New York, NY, USA, 4228–4232. https://doi.org/10.1145/2858036.2858559

[23] Gierad Laput, Eric Brockmeyer, Scott E. Hudson, and Chris Harrison. 2015. Acoustruments: Passive, Acoustically-Driven, Interactive Controls for Handheld Devices. In *Proceedings of the 33rd Annual ACM Conference on Human Factors in Computing Systems* (Seoul, Republic of Korea) *(CHI '15)*. Association for Computing Machinery, New York, NY, USA, 2161–2170. https://doi.org/10.1145/2702123.2702414

[24] SciKit Learn. 2025. ExtraTreesRegressor. https://scikit-learn.org/stable/modules/generated/sklearn.ensemble.ExtraTreesRegressor.html.

[25] Susan J. Lederman and Roberta L. Klatzky. 2009. Haptic perception: A tutorial. *Attention, Perception, & Psychophysics* 71, 7 (2009), 1439–1459.

[26] Darren Leigh, Clifton Forlines, Ricardo Jota, Steven Sanders, and Daniel Wigdor. 2014. High rate, low-latency multi-touch sensing with simultaneous orthogonal multiplexing. In *Proceedings of the 27th Annual ACM Symposium on User Interface Software and Technology* (Honolulu, Hawaii, USA) *(UIST '14)*. Association for Computing Machinery, New York, NY, USA, 355–364. https://doi.org/10.1145/2642918.2647353

[27] Yifan Li, Masaaki Fukumoto, Mohamed Kari, Tomoyuki Yokota, Takao Someya, Yoshihiro Kawahara, and Ryo Takahashi. 2025. Demo of picoRing mouse: ultra-low-powered wireless mouse ring with ring-to-wristband coil-based impedance sensing. In *Proceedings of the Extended Abstracts of the CHI Conference on Human Factors in Computing Systems (CHI EA '25)*. Association for Computing Machinery, New York, NY, USA, Article 707, 5 pages. https://doi.org/10.1145/3706599.3721183

[28] Rong-Hao Liang, Liwei Chan, Hung-Yu Tseng, Han-Chih Kuo, Da-Yuan Huang, De-Nian Yang, and Bing-Yu Chen. 2014. GaussBricks: magnetic building blocks for constructive tangible interactions on portable displays. In *Proceedings of the SIGCHI Conference on Human Factors in Computing Systems* (Toronto, Ontario, Canada) *(CHI '14)*. Association for Computing Machinery, New York, NY, USA, 3153–3162. https://doi.org/10.1145/2556288.2557105

[29] Rong-Hao Liang, Kai-Yin Cheng, Liwei Chan, Chuan-Xhyuan Peng, Mike Y. Chen, Rung-Huei Liang, De-Nian Yang, and Bing-Yu Chen. 2013. GaussBits: magnetic tangible bits for portable and occlusion-free near-surface interactions. In *Proceedings of the SIGCHI Conference on Human Factors in Computing Systems* (Paris, France) *(CHI '13)*. Association for Computing Machinery, New York, NY, USA, 1391–1400. https://doi.org/10.1145/2470654.2466185

[30] Rong-Hao Liang, Kai-Yin Cheng, Chao-Huai Su, Chien-Ting Weng, Bing-Yu Chen, and De-Nian Yang. 2012. GaussSense: attachable stylus sensing using magnetic sensor grid. In *Proceedings of the 25th Annual ACM Symposium on User Interface Software and Technology* (Cambridge, Massachusetts, USA) *(UIST '12)*. Association for Computing Machinery, New York, NY, USA, 319–326. https://doi.org/10.1145/2380116.2380157

[31] Rong-Hao Liang, Han-Chih Kuo, Miguel Bruns Alonso, and Bing-Yu Chen. 2016. GaussStudio: Designing Seamless Tangible Interactions on Portable Displays. In *Proceedings of the TEI '16: Tenth International Conference on Tangible, Embedded, and Embodied Interaction* (Eindhoven, Netherlands) *(TEI '16)*. Association for Computing Machinery, New York, NY, USA, 786–789. https://doi.org/10.1145/2839462.2854111

[32] Rong-Hao Liang, Han-Chih Kuo, Liwei Chan, De-Nian Yang, and Bing-Yu Chen. 2014. GaussStones: shielded magnetic tangibles for multi-token interactions on portable displays. In *Proceedings of the 27th Annual ACM Symposium on User Interface Software and Technology* (Honolulu, Hawaii, USA) *(UIST '14)*. Association for Computing Machinery, New York, NY, USA, 365–372. https://doi.org/10.1145/2642918.2647384

[33] Rong-Hao Liang, Han-Chih Kuo, and Bing-Yu Chen. 2016. GaussRFID: Reinventing Physical Toys Using Magnetic RFID Development Kits. In *Proceedings of the 2016 CHI Conference on Human Factors in Computing Systems* (San Jose, California, USA) *(CHI '16)*. Association for Computing Machinery, New York, NY, USA, 4233–4237. https://doi.org/10.1145/2858036.2858527

[34] Lars Lischke, Jürgen Grüninger, Khalil Klouche, Albrecht Schmidt, Philipp Slusallek, and Giulio Jacucci. 2015. Interaction Techniques for Wall-Sized Screens. In *Proceedings of the 2015 International Conference on Interactive Tabletops & Surfaces* (Madeira, Portugal) *(ITS '15)*. Association for Computing Machinery, New York, NY, USA, 501–504. https://doi.org/10.1145/2817721.2835071

[35] Chin-Yuan Lu, Han-Wei Hsieh, Rong-Hao Liang, Chi-Jung Lee, Ling-Chien Yang, Mengru Xue, Jr-Ling Guo, Meng-Ju Hsieh, and Bing-Yu Chen. 2021. Combining Touchscreens with Passive Rich-ID Building Blocks to Support Context Construction in Touchscreen Interactions. In *Proceedings of the 2021 CHI Conference on Human Factors in Computing Systems* (Yokohama, Japan) *(CHI '21)*. Association for Computing Machinery, New York, NY, USA, Article 506, 14 pages. https://doi.org/10.1145/3411764.3445722

[36] Yiyue Luo, Chao Liu, Young Joong Lee, Joseph DelPreto, Kui Wu, Michael Foshey, Daniela Rus, Tomás Palacios, Yunzhu Li, Antonio Torralba, et al. 2024. Adaptive tactile interaction transfer via digitally embroidered smart gloves. *Nature communications* 15, 1 (2024), 868.

[37] Guy Lüthi, Andreas Rene Fender, and Christian Holz. 2022. DeltaPen: A device with integrated high-precision translation and rotation sensing on passive surfaces. In *Proceedings of the 35th Annual ACM Symposium on User Interface Software and Technology*. 1–12.

[38] I. Scott MacKenzie. 1995. *Input devices and interaction techniques for advanced computing*. Oxford University Press, Inc., USA, 437–470.

[39] Tomer Moscovich and John F. Hughes. 2006. Multi-finger cursor techniques. In *Proceedings of Graphics Interface 2006* (Quebec, Canada) *(GI '06)*. Canadian

Information Processing Society, CAN, 1–7.
[40] Michael Ortner and Alex Zapp. 2025. Magpylib Documentation. Version 5.0.3. https://magpylib.readthedocs.io/en/stable/.
[41] Panasonic. 2012. Multi Function Switches/EVQWJN. https://www.alldatasheet.com/datasheet-pdf/view/1643682/PANASONIC/EVQWJN005.html.
[42] Farshid Salemi Parizi, Eric Whitmire, and Shwetak Patel. 2019. Auraring: Precise electromagnetic finger tracking. *Proceedings of the ACM on Interactive, Mobile, Wearable and Ubiquitous Technologies* 3, 4 (2019), 1–28.
[43] James Patten, Hiroshi Ishii, Jim Hines, and Gian Pangaro. 2001. Sensetable: a wireless object tracking platform for tangible user interfaces. In *Proceedings of the SIGCHI Conference on Human Factors in Computing Systems* (Seattle, Washington, USA) *(CHI '01)*. Association for Computing Machinery, New York, NY, USA, 253–260. https://doi.org/10.1145/365024.365112
[44] Bo NJ Persson. 2001. Theory of rubber friction and contact mechanics. *The Journal of Chemical Physics* 115, 8 (2001), 3840–3861.
[45] Florian Perteneder, Kathrin Probst, Joanne Leong, Sebastian Gassler, Christian Rendl, Patrick Parzer, Katharina Fluch, Sophie Gahleitner, Sean Follmer, Hideki Koike, and Michael Haller. 2020. Foxels: Build Your Own Smart Furniture. In *Proceedings of the Fourteenth International Conference on Tangible, Embedded, and Embodied Interaction* (Sydney NSW, Australia) *(TEI '20)*. Association for Computing Machinery, New York, NY, USA, 111–122. https://doi.org/10.1145/3374920.3374935
[46] PyTorch. 2025. LSTM. https://docs.pytorch.org/docs/stable/generated/torch.nn.LSTM.html.
[47] Jun Rekimoto. 2002. SmartSkin: an infrastructure for freehand manipulation on interactive surfaces. In *Proceedings of the SIGCHI Conference on Human Factors in Computing Systems* (Minneapolis, Minnesota, USA) *(CHI '02)*. Association for Computing Machinery, New York, NY, USA, 113–120. https://doi.org/10.1145/503376.503397
[48] Hugo Romat, Andreas Fender, Manuel Meier, and Christian Holz. 2021. Flashpen: A high-fidelity and high-precision multi-surface pen for virtual reality. In *2021 IEEE Virtual Reality and 3D User Interfaces (VR)*. IEEE, 306–315.
[49] Munehiko Sato, Ivan Poupyrev, and Chris Harrison. 2012. Touché: enhancing touch interaction on humans, screens, liquids, and everyday objects. In *Proceedings of the SIGCHI Conference on Human Factors in Computing Systems* (Austin, Texas, USA) *(CHI '12)*. Association for Computing Machinery, New York, NY, USA, 483–492. https://doi.org/10.1145/2207676.2207743
[50] Martin Schmitz, Florian Müller, Max Mühlhäuser, Jan Riemann, and Huy Viet Viet Le. 2021. Itsy-Bits: Fabrication and Recognition of 3D-Printed Tangibles with Small Footprints on Capacitive Touchscreens. In *Proceedings of the 2021 CHI Conference on Human Factors in Computing Systems* (Yokohama, Japan) *(CHI '21)*. Association for Computing Machinery, New York, NY, USA, Article 419, 12 pages. https://doi.org/10.1145/3411764.3445502
[51] Orit Shaer and Eva Hornecker. 2010. TangibleUserInterfaces: Past, Present, and Future Directions. *Found. Trends Hum.-Comput. Interact.* 3, 1–2 (Jan. 2010), 1–137. https://doi.org/10.1561/1100000026
[52] Miika Silfverberg, I. Scott MacKenzie, and Tatu Kauppinen. 2001. An isometric joystick as a pointing device for handheld information terminals. In *Proceedings of Graphics Interface 2001* (Ottawa, Ontario, Canada) *(GI '01)*. Canadian Information Processing Society, CAN, 119–126.
[53] Lanny S. Smoot. 2023. Omni-directional treadmill.
[54] Nobuyuki Umezu and Hideki Bando. 2025. Augmented Karuta: Interactive Playing Cards on the Floor for Learning Local Culture. In *2025 IEEE International Conference on Artificial Intelligence and eXtended and Virtual Reality (AIxVR)*. 331–335. https://doi.org/10.1109/AIxVR63409.2025.00063
[55] Irmandy Wicaksono, Lancelot Blanchard, Sam Chin, Cristian Colon, and Joseph Paradiso. 2024. KnitworkVR: Dual-reality Experience through Distributed Sensor-Actuator Networks in the Living Knitwork Pavilion. In *SIGGRAPH Asia 2024 Art Papers (SA '24)*. Association for Computing Machinery, New York, NY, USA, Article 12, 7 pages. https://doi.org/10.1145/3680530.3695456
[56] Irmandy Wicaksono, Don Derek Haddad, and Joseph Paradiso. 2022. Tapis Magique: Machine-knitted Electronic Textile Carpet for Interactive Choreomusical Performance and Immersive Environments. In *Proceedings of the 14th Conference on Creativity and Cognition* (Venice, Italy) *(C&C '22)*. Association for Computing Machinery, New York, NY, USA, 262–274. https://doi.org/10.1145/3527927.3531451
[57] Te-Yen Wu, Lu Tan, Yuji Zhang, Teddy Seyed, and Xing-Dong Yang. 2020. Capacitivo: Contact-Based Object Recognition on Interactive Fabrics using Capacitive Sensing. In *Proceedings of the 33rd Annual ACM Symposium on User Interface Software and Technology* (Virtual Event, USA) *(UIST '20)*. Association for Computing Machinery, New York, NY, USA, 649–661. https://doi.org/10.1145/3379337.3415829
[58] Youcan Yan, Zhe Hu, Zhengbao Yang, Wenzhen Yuan, Chaoyang Song, Jia Pan, and Yajing Shen. 2021. Soft magnetic skin for super-resolution tactile sensing with force self-decoupling. *Science Robotics* 6, 51 (Feb. 2021), eabc8801. https://doi.org/10.1126/scirobotics.abc8801
[59] Kentaro Yasu. 2019. Magnetact: Magnetic-sheet-based Haptic Interfaces for Touch Devices. In *Proceedings of the 2019 CHI Conference on Human Factors in Computing Systems* (Glasgow, Scotland Uk) *(CHI '19)*. Association for Computing Machinery, New York, NY, USA, 1–8. https://doi.org/10.1145/3290605.3300470
[60] Kentaro Yasu. 2024. MagneSwift: Low-Cost, Interactive Shape Display Leveraging Magnetic Materials. In *Proceedings of the 2024 CHI Conference on Human Factors in Computing Systems* (Honolulu, HI, USA) *(CHI '24)*. Association for Computing Machinery, New York, NY, USA, Article 863, 11 pages. https://doi.org/10.1145/3613904.3642058
[61] Neng-Hao Yu, Liwei Chan, Seng-Yong Lau, Sung-Sheng Tsai, I-Chun Hsiao, Dian-Je Tsai, Fang-I Hsiao, Lung-Pan Cheng, Mike Y. Chen, Polly Huang, and Yi-Ping Hung. 2011. TUIC: enabling tangible interaction on capacitive multi-touch displays. *Proceedings of the SIGCHI Conference on Human Factors in Computing Systems* (2011). https://api.semanticscholar.org/CorpusID:213299
[62] Sen Zhang, Yuxuan Miao, Jazlin Taylor, and Yiyue Luo. 2025. MagTex: Machine-Knitted Magnetoactive Textiles for Bidirectional Human–Machine Interface. In *Proceedings of the 38th Annual ACM Symposium on User Interface Software and Technology (UIST '25)*. ACM, Busan, Republic of Korea. https://doi.org/10.1145/3746059.3747648
[63] Yang Zhang, Gierad Laput, and Chris Harrison. 2017. Electrick: Low-Cost Touch Sensing Using Electric Field Tomography. In *Proceedings of the 2017 CHI Conference on Human Factors in Computing Systems* (Denver, Colorado, USA) *(CHI '17)*. Association for Computing Machinery, New York, NY, USA, 1–14. https://doi.org/10.1145/3025453.3025842